Experimental Investigations on PV Powered SVM-DTC Induction Motor without AC Phase Current Sensors

T. Muthamizhan [#1], R. Ramesh [#2]

[#] Department of Electrical and Electronics Engineering, College of Engineering Guindy, Anna University, Chennai 600 025, Tamil Nadu, India.

[1]thamizh@annauniv.edu

[2]rramesh@annauniv.edu

Abstract—The paper presents a low-cost, phase-current reconstruction algorithm for space vector modulated direct torque controlled induction motor using the information obtained from only one shunt resistor which is in series with low side switches in a conventional three-phase inverter. The aim is to develop a low-cost high - performance induction motor drive. It uses the dc-link voltage and dc current to reconstruct the stator currents needed to estimate the motor flux and the electromagnetic torque. Photovoltaic arrays convert solar power to dc electric power; uses chopper and dc-ac inverter to fed three phase Induction Motor. The chopper used here is current fed full bridge boost dc-dc converter, which is preferred and extensively used in high voltage applications and advantageous over voltage fed converters. The inverter switches are controlled by PWM techniques obtained from SVM-DTC of IM. The experimental investigations are given to prove the ability of the proposed scheme of reproducing the performances of a SVM- DTC IM drive.

Keyword - Photovoltaic, Zero Current Switching, SVM, DTC, Induction Motor.

I. INTRODUCTION

Adjustable-speed drives are widespread electromechanical systems suitable for a remarkable range of industrial applications. When high dynamic performance and precision control are required for an induction motor in a wide speed range, the speed must normally be measured. Direct torque control (DTC) is a powerful control scheme for the control of induction motor (IM) drives, uses hysteresis comparators for the control of both stator flux magnitude and electromagnetic torque. The control scheme ideally keeps both controlled parameters within the hysteresis bands and results in a non-constant switching frequency. When DTC is implemented using a two-level voltage source inverter (VSI), eight different voltage vectors, of which only six are classified as active voltage vectors, can be applied to the machine. The integration of space vector modulation (SVM) has shown to be an effective method to lower the ripples in the torque and flux. SVM-based DTC schemes calculate an optimal reference voltage vector applied to the machine using SVM. A typical configuration of a batteryless photovoltaic pumping system is shown in Fig. 1. The system comprises the following components: 1) photovoltaic panels; 2) dc-dc converter; 3) dc-ac inverter; 4) induction motor; and 5) MPPT System. The design of an effective photovoltaic pumping system without the use of a battery bank represents a significant challenge. The PV module characteristics and the issue of maximum power point tracking (MPPT) have been addressed in different ways in the literature [1], [7] - [10]. There are advantages in avoiding the use of lead-acid batteries, which are heavy and expensive, have one-fifth of the life time of the photovoltaic panel. However, the absence of the batteries does not compromise the power conversion chain from the photovoltaic panel to induction motor. The fixed frequency phase-shift control enables the implementation of ZCS for all converter switches. The switches must provide a reverse-voltage blocking capability and hence they have to be constructed by means of an insulated-gate bipolar transistor (IGBT) or MOSFET in series with reverse-voltage blocking diodes. Current-fed zero-voltage transition PWM converter use auxiliary network and hence all the power switches are zero-voltage switched or zero-current switched [2], [4], [20]. The space vector pulse width modulation (SVPWM) method an advanced computation-intensive PWM method for variable frequency drive applications have superior performance characteristics, it has been finding widespread application in recent years [6], [11], [13], [19]. Sensor less space vector pulse width modulated direct torque controlled induction motor drive utilizing modified stator flux estimation logic has been proposed in literature [5], [14], [18]. Sensorless speed control of Induction Motor include speed and flux estimations and hence increase the computational complexity and the time to estimate the speed and flux of Induction Motor. Direct torque control (DTC) techniques for voltage inverter-fed induction motors and techniques such as switching-table-based hysteresis DTC, direct self control, constant-switching-frequency DTC with space-vector modulation (DTC-SVM) are discussed [3], [15]. Photovoltaic arrays, comprising a converter and an induction motor, design principles and the optimization of a sensorless induction motor drive system are discussed [16], [17].

II.PHOTOVOLTAIC SYSTEM.

The conversion of solar energy into electricity using photovoltaic system is the valuable way of producing the alternative energy. One of the most promising applications of photovoltaic energy is new design of an efficient batteryless pumping. However, the absence of batteries does not compromise the efficiency of the power conversion chain. Fig. 2 shows the equivalent circuit of the solar cell. The equivalent circuit of a solar cell is a current source in parallel with an inverted diode. The output of the current source is directly proportional to the sunlight falling on the cell (photocurrent Iph). During cloudy day or at night, the solar cell is not active and hence it works as a diode, i.e. a p-n junction. It produces neither a current nor a voltage. However, if it is connected to an external supply (large voltage) it generates a current I_d, called diode (D) current or dark current. The diode determines the I-V characteristics of the cell. The V-I characteristic of a single-junction P-N under illumination can be written as follows:

$$I = I_L - I_d \tag{1}$$

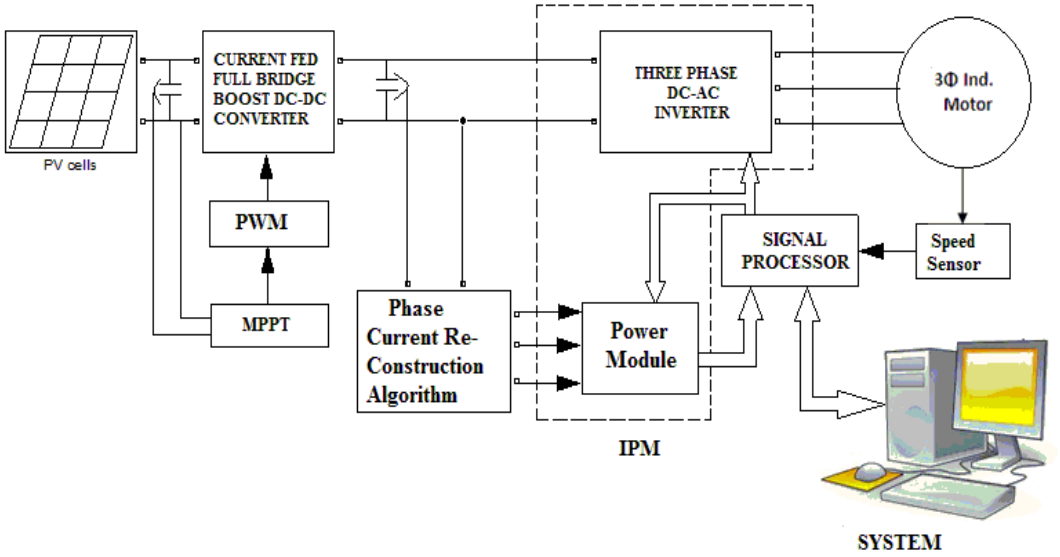

Fig.1 Block diagram of SVM-DTC Induction Motor with Phase Current reconstruction algorithm

$$I = I_L - I_0\left[\exp\left(\frac{q(V + IR_S)}{nkT}\right) - 1\right] \tag{2}$$

Where the net current is the difference of photocurrent and diode current, V is the voltage, T is the absolute temperature and R_S is the series resistance inside each cell in connection between the cells. The shunt resistance R_{sh} is neglected. Here, n, k, T, q, V and I_0 are the diode quality factor, Boltzmann constant [k = 1.38 × 10^{-23} (j/K)], absolute temperature of SC [K], electron charge [1.6 × 10^{-19}C], voltage across the cell, and the dark saturation current that varies greatly depending on the temperature, respectively. If the output current assumed as zero, open circuit voltage (V_{OC}) is determined by

$$V_{OC} = \frac{nkT}{q}\ln\frac{I_L + I_0}{I_0} \approx \frac{nkT}{q}\ln\frac{I_L}{I_0} \tag{3}$$

and I_0 can be neglected since it is very small compared to I_L. The most efficient operation point of cell is (A) and called as maximum power point (MPP). Output power (P_{max}) and efficiency (η_{max}) values at this point are equal to

$$P_{max} = I_{max}.V_{max} \tag{4}$$

$$\eta_{max} = \frac{P_{max}}{p_{in}} = \frac{P_{max}}{A.G_a} \tag{5}$$

In the above equations, A is area of photovoltaic array [m^2] and Ga represents photovoltaic array ambient solar radiation in W/m^2. Another criterion of I-V characteristic is fill factor (FF), determine the quality of Solar Cells which must be 0.7 or greater. Mathematically, FF can be expressed by the equation:

$$FF = \frac{P_{max}}{V_{OC} I_{SC}} = \frac{V_{max} . I_{max}}{V_{OC} I_{SC}} \quad (6)$$

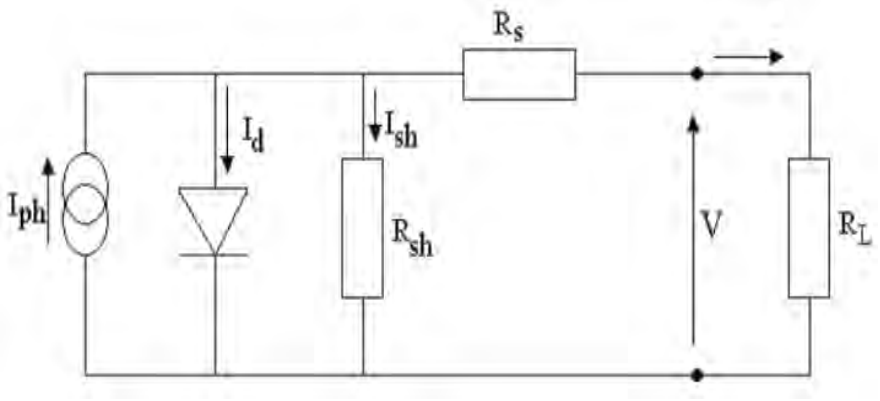

Fig. 2 Equivalent circuit of the solar cell

A single shunt diode was used with the diode quality factor set to achieve the best curve match. Solar cells are usually connected in series, in the modules, creating an additive voltage and in parallel to yield higher amperage. Modules are then interconnected, in series and parallel to create the desired peak dc voltage and current. Fig. 3 shows the Power – Voltage (P-V) and Voltage - Current (V-I) characteristics of single PV cell.

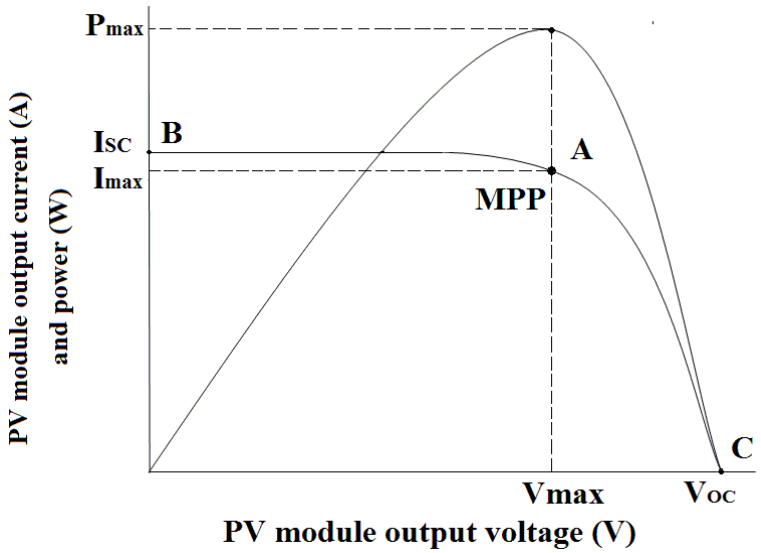

Fig. 3 Characteristics of a PV cell

Parameters	Rating
STC Power Rating Pmp	75 W
Open Circuit Voltage Voc	21.0 V
Short Circuit Current Isc	5.00 A
Voltage at Maximum Power Vmp	17.1 V
Current at Maximum Power Imp	4.39 A
Panel Efficiency	11.6%
Fill Factor	71.4%
Maximum System Voltage Vmax	600 V

Fig. 4 USP75 M5C01 solar panel and its specification

Fig. 5 Solar array setup for 1kW

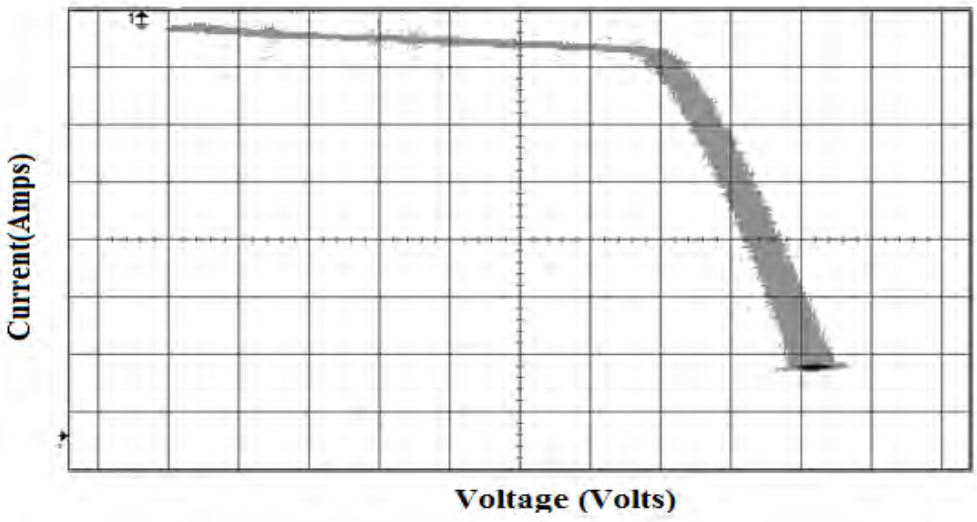

Y axis : 1.5 Amps/div, X axis : 12 Volts/div

Fig. 6 V-I Curve of the 1KW solar array at 1000w/m^2

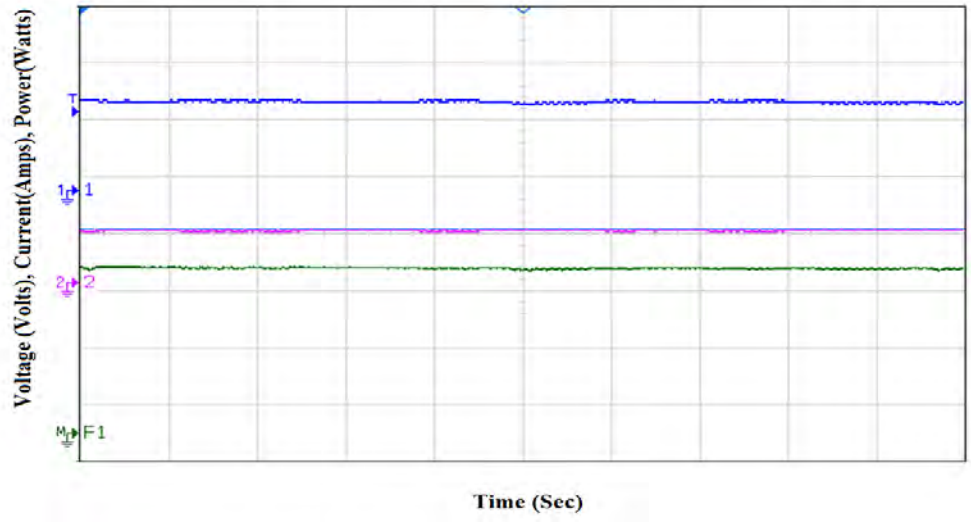

Y axis: 100 Volts/div, 10 Amps/div, 500Watts/div

Fig. 7 Voltage, current and power curve of 1kW rating solar array

Fig. 4 shows a solar panel and its specification. PV cells are connected together to make panel consisting of 36 PV cells, which generates open circuit voltage of 21V and short circuit current of 5A and a maximum power of 75W, depending on temperature and solar irradiation. Fig. 5 shows the 1 KW solar array setup to yield an open circuit voltage of 120V-180V and Fig. 6 shows the V-I curve of the solar array at an irradiance of 1kW/m^2at STC. Fig. 7 shows the Voltage, Current and Power characteristics curve of 1kW rating solar array at an irradiance level of 1kW/m^2

III.MAXIMUM POWER POINT TRACKING

Maximum power point (MPP) varies depending on the angle of sunlight on the surface of the panel and cell temperature. Hence, the operating point of the load is not always MPP of PV system. Therefore, in order to supply reliable energy to the load, PV systems are designed to include more than the required number of modules. The solution to this problem is that switching power converters are used, that is called maximum power point tracker (MPPT). The aim of MPPT is to regulate the operating voltage of PV panel to the voltage at MPP. Hence, MPPT adjusts the output power of inverter or dc/dc converter. If the PV output voltage is higher than MPP voltage, then transferred power to the load or network is increased, otherwise, it is decreased. Efficiency is the important parameter of an MPPT algorithm and is the ratio of the output power of PV system with MPPT to the output power at true maximum power point. It was obtained as a result of experimental studies that MPPT and it varies depending on cell temperature and fill factor. In the most general sense, MPPT techniques can be grouped under two headings as direct and indirect systems. In Direct MPPT Algorithms, the optimal operating point is determined by measurement of PV panel current, voltage or power. Therefore, these methods affected the performance changes in time due to various reasons and can make a more accurate tracking. One method used in MPP Tracking is the most well-known method called hill-climbing algorithm. Here, operating voltage is changed periodically in small steps, and the increase in module power or current is measured. So, increases or the standing start point of decreases is determined and accepted as the instantaneous operating point. If the power or current increases depending on the voltage rising of each step, tracking direction is forward, otherwise it is continued backwards. Maximum power point is determined with this way, and operating point makes an oscillation around real MPP. The “Hill Climbing” algorithm can be confused, and track the MPP in the wrong direction, in case of rapidly changing atmospheric conditions, when the change in PV power caused by change in irradiance is larger than the change in PV power as a function of the perturbation. The “Hill Climbing” will not be confused, if and only if

$$| \Delta P_u | > | \Delta P_g | \tag{7}$$

where ΔP_u is the change in power as function of change in voltage, and ΔPg is the change in power as function of change in irradiance.

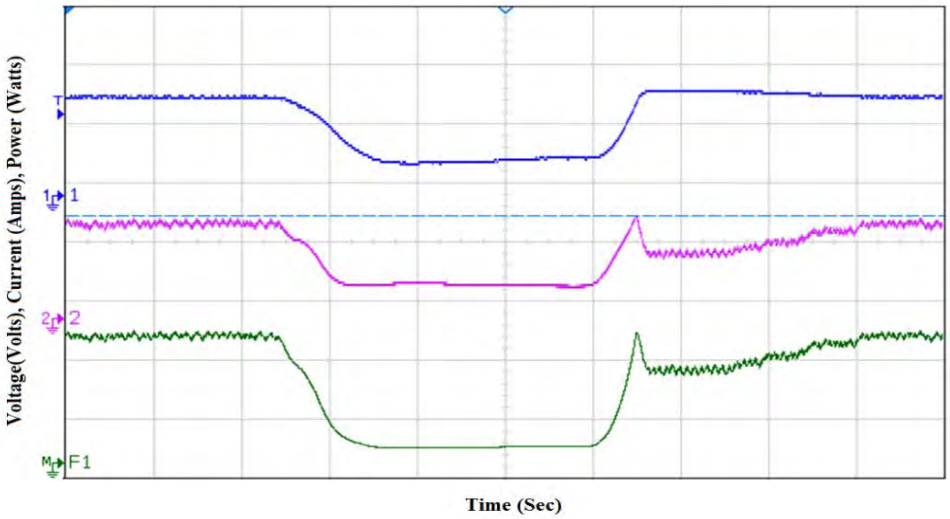

Y axis : 100 Volts/div, 10 Amps/div, 500Watts/div

Fig. 8 For a step irradiance change, the corresponding change in voltage, current and power waveforms by applying hill climbing MPPT

The hill climbing MPPT is optimized in respect with the sampling interval (T_a) and minimum step size (ΔV_d) in order to follow a certain irradiance ramp (dg/dt). The approach is based on a second-order Taylor approximation of the PV model including resistive parts. In the Fig. 3, if operating point of load is on the left of MPP, in other words if the module works as a current source, the error signal can be written as

$$\frac{\partial P_{module}}{\partial V_{module}} < 0 \Rightarrow M = M - \Delta M \quad (8)$$

In the opposite case, PV module acts as a voltage source, and error signal (M) is calculated as

$$\frac{\partial P_{module}}{\partial V_{module}} > 0 \Rightarrow M = M + \Delta M \quad (9)$$

At Maximum power point, error will be zero and expression is written as follows:

$$\frac{\partial P_{module}}{\partial V_{module}} = 0 \Rightarrow M = M \; or \; \Delta M = 0 \quad (10)$$

It is proved that the "Hill Climbing" algorithm is the one of the best method to extract the maximum power and hence this paper uses hill climbing algorithm to extract the maximum power. Fig. 8 shows the voltage, current and power waveforms and their corresponding change for a step irradiance change, by applying hill climbing MPPT and Fig. 9 shows the flowchart of the Hill Climbing MPPT algorithm.

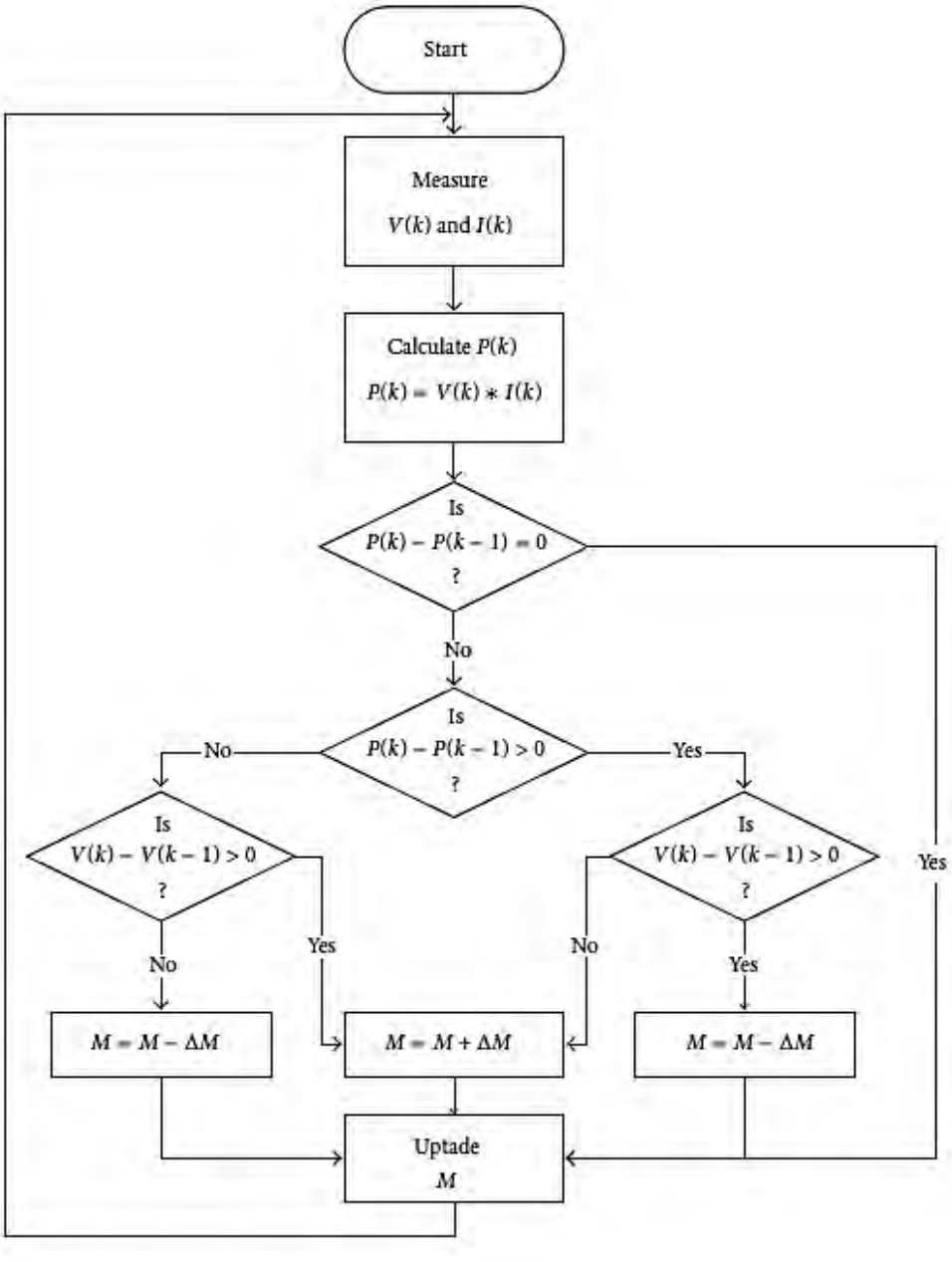

Fig. 9 Flowchart for the "Hill Climbing" MPPT algorithm

IV.CURRENT FED FULL-BRIDGE BOOST DC-DC CONVERTER

Power conversion for photovoltaic (PV) applications, as opposed to more conventional dc–dc converter configurations, requires an adaptable system that is capable of responding to a wide range of input voltage and current conditions. PV voltage varies significantly with panel construction and operating temperature, while the PV current changes largely due to solar irradiance and shading conditions. Current fed converters shown in Fig. 10 are preferred and extensively used in high voltage applications since it is advantageous than the voltage fed converters. A very high turns–ratio transformer is used to achieve a high output voltage in high voltage applications. The disadvantage of using large turns ratio transformer is the parasitic components (parasitic capacitance and leakage inductance) generate high voltage and current spikes, results in switching losses in the power devices, which has been overcome by ZCS operation. Constant on-time control methodology is utilized to achieve ZCS and a variable frequency control scheme is used to regulate the output voltage. The solar panel output in the range of 120V-180V is connected to the current fed full bridge boost dc-dc converters.

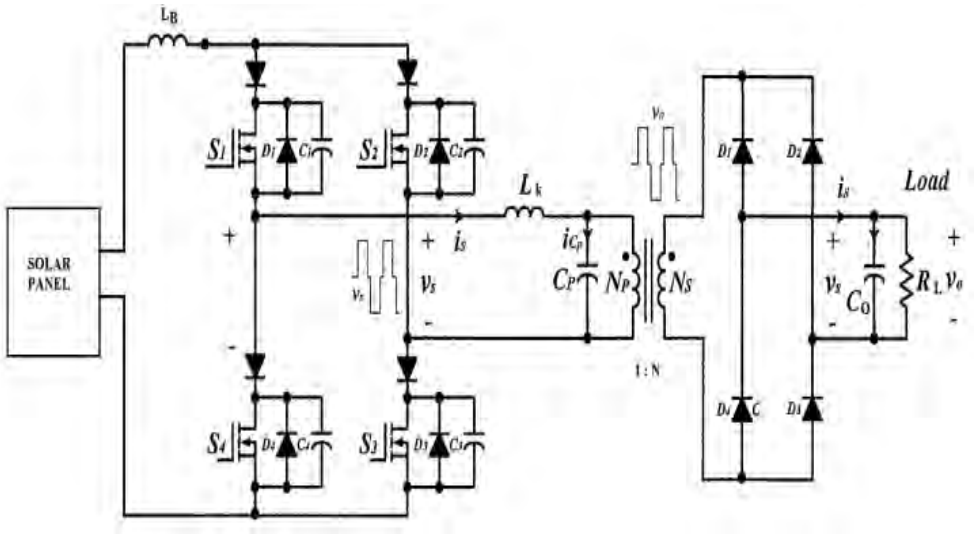

Fig. 10 Current fed full-bridge boost dc-dc converter.

Input Voltage : V=120V-180V (120V@ Maximum Power)

Input Power : 1 KW

Output Voltage: 600 V

A. *Design of Inductor:*

Let the voltage across the input side of the full bridge is 200V

The duty ratio is calculated as $\delta_{T\min}$ = 0.1 and $\delta_{T\max}$ = 0.4

The inductor value is calculated as

$$L \geq \frac{V_o\,\delta_{T\min}\,(1-\delta_{T\min})}{\Delta I_L\, f} \geq \frac{200*0.1*0.9}{1.85*18*10^3} \geq 0.541\mu H \tag{11}$$

Let us select EE 55/21 Ferrite core

Number of turns

$$N = \frac{L\,I_P*10^4}{B_m\,A_e} = \frac{541*10^{-6}*8.33*1.1*10^4}{0.3*3.51} = 47\,Turns \tag{12}$$

= 47 Turns of 16 SWG

Air gap value

$$\delta = \frac{\mu_o N\,I_P}{B_m} = \frac{1.257*10^{-3}*61*8.3*1.1}{0.3} = 1.8\,mm \tag{13}$$

I_P - Peak Currents

A_e - Effective Core Area

TABLE I
INDUCTOR DESIGN VALUES

Component	Design
Core	Ferrite EE 55 / 21
Coil	47 Turns of 16 SWG
Air gap	0.9 mm

SWG : Standard Wire Gauge

Table I shows the design values of the input boost inductor of the current fed full bridge boost dc-dc converter.

B. ***Design of High Frequency Transformer:***

Turns ratio of the high frequency transformer n is $n = \frac{N_s}{N_P}$, where N_S is the number of turns in the primary and N_P is the number of turns in the secondary.

$$n = \frac{V_{o\max} + V_F + V_{LS}}{\delta_{T\max} V_{i\min}} = \frac{600 + 4 + 2}{0.4 * 200} = 3.78 \quad (14)$$

V_F = Forward voltage drop of the diode

V_{LS} = Voltage drop in the primary side of the Transformer

Number of turns in the Primary side.

$$N_S \geq \frac{\delta_{T\max} * V_{P\max} * n * 10^4}{f * A_{\min} * 2 * B} \geq \frac{0.8 * 200 * 10^4}{18000 * 5.32 * 0.3} = 56 Turns \quad (15)$$

N_{PY} = 56 Turns

N_{SY} = 56 * 3.78 = 212 Turns

TABLE II
HIGH FREQUENCY TRANSFORMER DESIGN

Component	Design
Core	EE65/25
Coil	N_{PY} =56 Turns of 18 SWG
	N_{SY} = 212 Turns of 22 SWG

Table II shows the design values of the high frequency transformer in the current fed full bridge boost dc-dc converter. The current through the inductor of the current fed full bridge boost dc-dc converter is as shown in the Fig. 11.

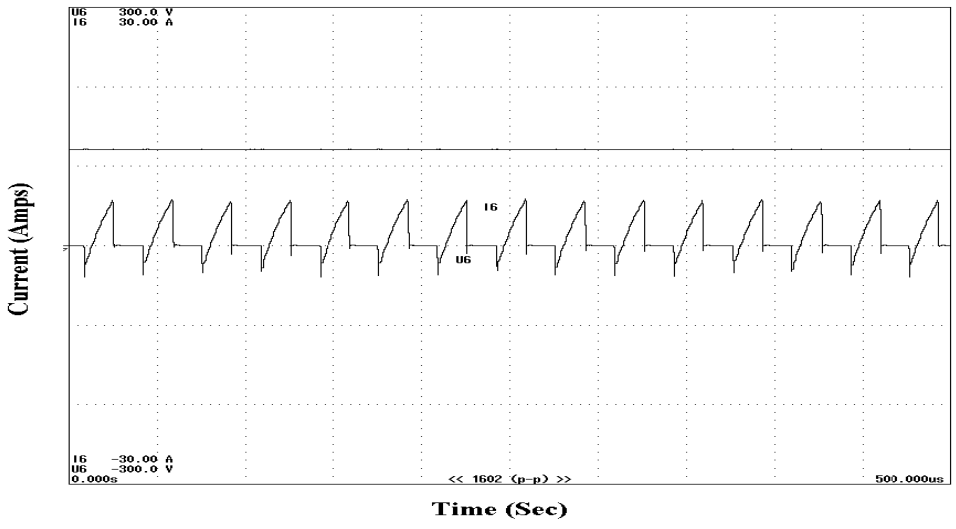

Fig. 11 Inductor current waveform of the current fed full-bridge boost dc-dc converter

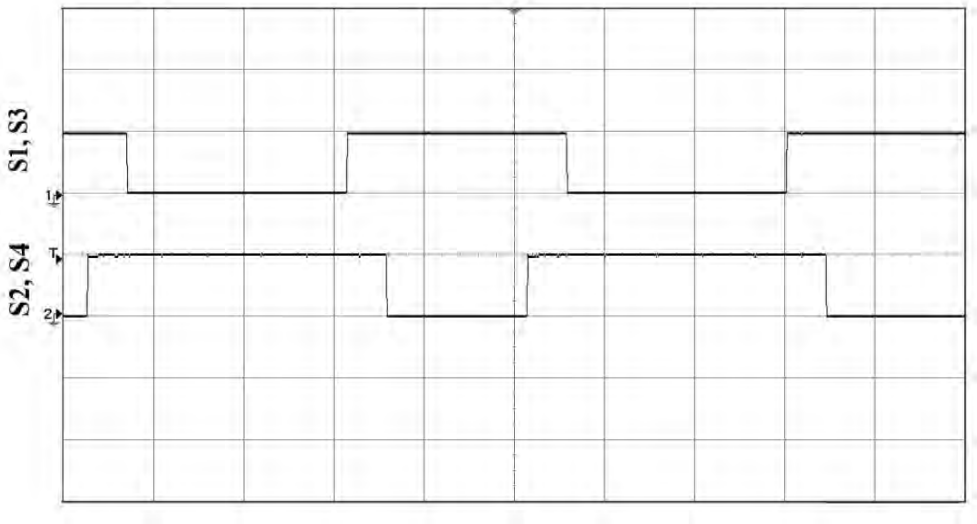

Fig. 12 Pulse to the current fed full-bridge boost converter

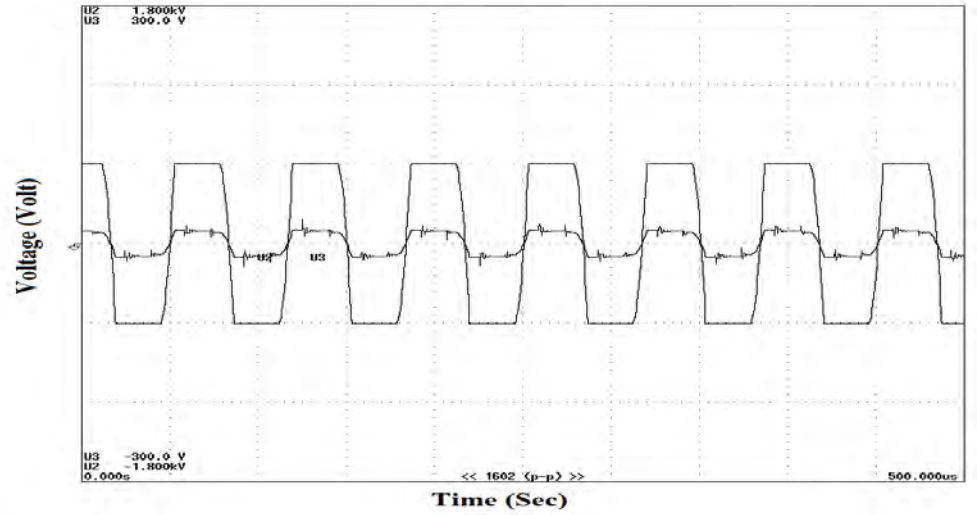

Fig. 13 Input and output voltage across the high frequency transformer

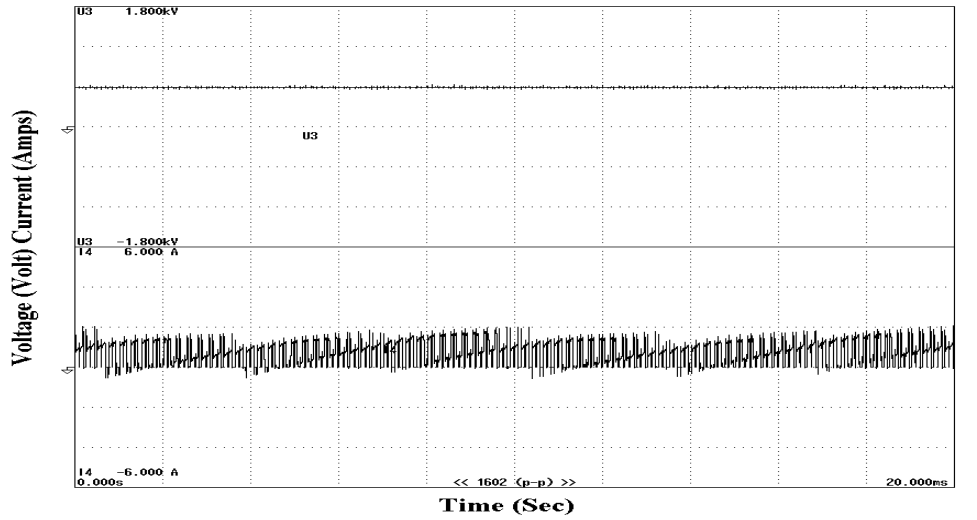

Fig. 14 dc voltage and dc current to three phase inverter

Pulses are applied to the switches S_1, S_3 and S_2, S_4 are as shown in the Fig. 12 to achieve zero current switching across the switches of the full bridge boost dc-dc converter. Fig. 13 shows the input voltage and the

output voltage at the high frequency transformer of the dc-dc converter. The dc voltage and the current measured at the output of the current fed full bridge boost dc-dc converter are as shown in the Fig. 14.

V. SVM-DTC INDUCTION MOTOR

DTC is one of the methods used in variable frequency drives, to control the torque and hence the speed of three-phase ac motors by calculating the motor's magnetic flux and torque based on the measured voltage and current of the motor. The DTC method operates in the stationary reference frame and acts directly on the inverter switches to produce the necessary stator voltages. Hysteretic controllers are used to constrain the electrical torque and stator flux magnitude within certain bounds. The major problem in a DTC-based motor drive is the presence of ripples in the motor-developed torque and stator flux. Generally, there are two main techniques to reduce the torque ripples. One method is multilevel inverter and second method is to use Space vector modulation. The multilevel inverter will provide more precise control of motor torque and flux however, the complexity and cost of the controller increase comparably. The space vector modulation strategy is used in the DTC Method. Space vector techniques have several advantages that are offering better dc bus utilization, lower torque ripple, lower total harmonic distortion in the ac motor current, lower switching loss, and easier to implement in the digital systems. However, the performance of DTC strongly depends on the quality of the estimation of the actual stator flux and torque.

The main features of DTC can be summarized as follows.

- DTC operates with closed torque and flux loops without current controllers.
- DTC needs stator flux and torque estimation and it is not sensitive to rotor parameters.
- DTC is inherently a motion-sensor less control method.
- DTC has a simple and robust control structure;

A low-cost and simple phase-current reconstruction algorithm for three-phase IM under DTC using the information obtained from only one shunt resistor in series with low side switches in a conventional three-phase inverter. The aim is to develop a low-cost high-performance IM drive. The proposed algorithm is robust and very simple and uses the dc current to reconstruct the stator currents needed to estimate the motor flux and the electromagnetic torque. A theoretical concept is developed, the modified look-up table is presented, and current-access tables are designed and used in the phase-current reconstruction. The stator flux vector and the electromagnetic torque are directly calculated from the voltage and the current derived from a single dc-link voltage sensor from a voltage divider network and a single dc-link current sensor by using a shunt resistor. The phase currents are estimated by two dc-link current measurement processes. This algorithm does not require additional computation burden or other motor parameter knowledge.

The dc output voltage is filtered with a bulk capacitor and the dc voltage is given as input to the three phase inverter connected to the three phase induction motor. Here PI controller is used to tune the speed error which is used to generate the torque reference signal. Classical controllers with limitations have been used to control induction machines in achieving desired dynamic response. One modification of the basic DTC is used for estimating the three-phase currents from a single dc-link current sensor. On the modification, the need of an additional current sensor requirement is minimized. The six voltage vector is applied at each cycle period, for prefixed time intervals for the Space Vector Modulation (SVM) technique.

TABLE III
DTC SWITCHING TABLE

Sector		1	2	3	4	5	6
$C_{Ø}$ = -1	c_T = -1	V_2	V_3	V_4	V_5	V_6	V_1
	c_T = 0	V_7	V_0	V_7	V_0	V_7	V_0
	c_T = +1	V_6	V_1	V_2	V_3	V_4	V_5
$C_{Ø}$ = +1	c_T = -1	V_3	V_4	V_5	V_6	V_1	V_2
	c_T = 0	V_0	V_7	V_0	V_7	V_0	V_7
	c_T = +1	V_5	V_6	V_1	V_2	V_3	V_4

By using this modulation strategy, the voltage vectors are synthesized with respect to those used in the basic DTC technique from −30◦ to 30◦. The DTC switching table is tabulated in Table III. The PWM generated by the space vector pulse width modulation techniques for the classical DTC is as shown in the Fig. 17. The output voltage for various switching patterns can be obtained by considering an example of Space voltage V_6 (state 101); the output voltages V_{an}, V_{bn} and V_{cn} are obtained by the equivalent circuit as shown in Fig. 15. The phase voltages and currents are reconstructed using the dc-link voltage, dc-link current and the voltages applied to the

switches. The phase voltages and phase currents of the stator of three phase inductor motor are reconstructed using dc-link voltage, dc-link current and the voltage applied to the inverter switches.

The output voltages V_{an}, V_{bn} and V_{cn} can be calculated using the Equation 16 and are given as follows:

$$Z_{eq} = \frac{3Z}{2} \tag{16}$$

$$V_{an} = V_{cn} = V_{dc} \frac{z}{2} \Big/ 3\frac{z}{2} = \frac{V_{dc}}{3} \tag{17}$$

$$V_{bn} = -V_{dc}.z \Big/ 3\frac{z}{2} = \frac{-2V_{dc}}{3} \tag{18}$$

where V_{dc} is the dc link voltage. Similarly we can calculate the values of V_{an}, V_{bn} and V_{cn} for the other five nonzero states. V_0 and V_1 are the zero states of the space voltage. The inverter switching states is tabulated in Table IV and the parameters of the induction motor are tabulated in Table V.

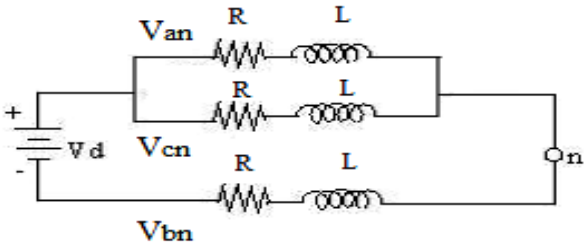

Fig. 15 Equivalent circuit to find V_{an}, V_{bn} and V_{cn}

TABLE IV
SUMMARY OF INVERTER SWITCHING STATES

Name	C	B	A	V_{an}	V_{bn}	V_{cn}
V_0	0	0	0	0	0	0
V_1	0	0	1	$2V_{dc}$ / 3	$-V_{dc}$ / 3	$-V_{dc}$ / 3
V_2	0	1	0	V_{dc} / 3	V_{dc} / 3	$-2V_{dc}$ / 3
V_3	0	1	1	$-V_{dc}$ / 3	$2V_{dc}$ / 3	$-V_{dc}$ / 3
V_4	1	0	0	$-2V_{dc}$ / 3	V_{dc} / 3	V_{dc} / 3
V_5	1	0	1	$-V_{dc}$ / 3	$-V_{dc}$ / 3	$2V_{dc}$ / 3
V_6	1	1	0	V_{dc} / 3	$-2V_{dc}$ / 3	V_{dc} / 3
V_7	1	1	1	0	0	0

TABLE V
PARAMETERS OF THE INDUCTION MOTOR

Parameters	Ratings
Rated power	1 HP
Rated voltage	415V
Rated speed	1440 RPM
Pole pairs	2
Stator resistance	19.35 Ω
Rotor resistance	8.43 Ω
Stator leakage inductance	32 mH
Rotor leakage inductance	32 mH
Air gap inductance	0.601 H
Rotor time constant (J)	0.0051Kg.m^2
Friction factor(F)	0.06 Nm.s

The phase voltage and phase currents are reconstructed by the algorithm using dc link voltage and dc link current. Fig. 16 shows the line voltage and phase current when no loads are connected to the shaft. Fig. 17 shows the pulse generated by the Sparton 3E FPGA kit for the three phase inverter switches is as shown. Fig. 18

shows the forward and reverse flux angle, when the speed is forward and reversed and is plotted in the same graph. Fig. 19 shows the speed and Torque characteristics of the induction motor when load is applied, the torque increase suddenly and the speed decreseas and settles down at the set speed in 2 seconds.

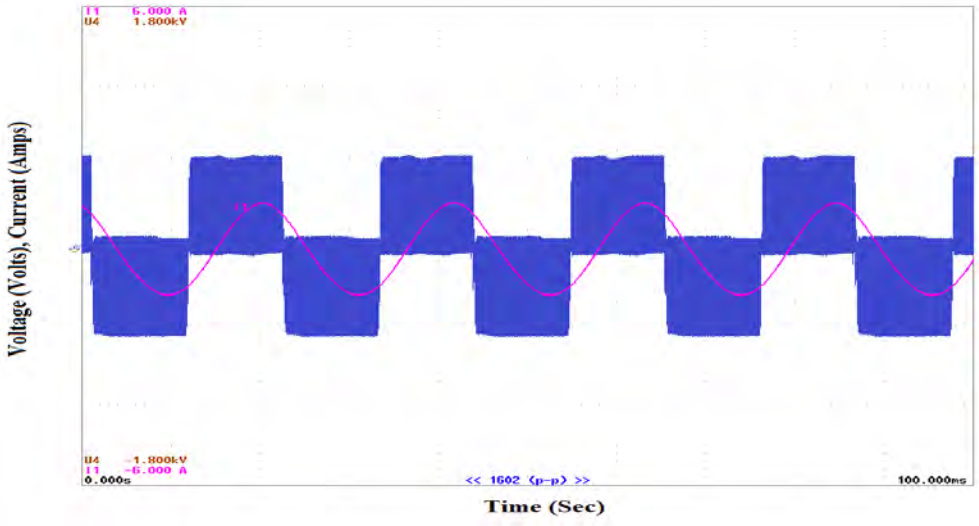

Fig. 16 Line voltage and phase current at no-load condition

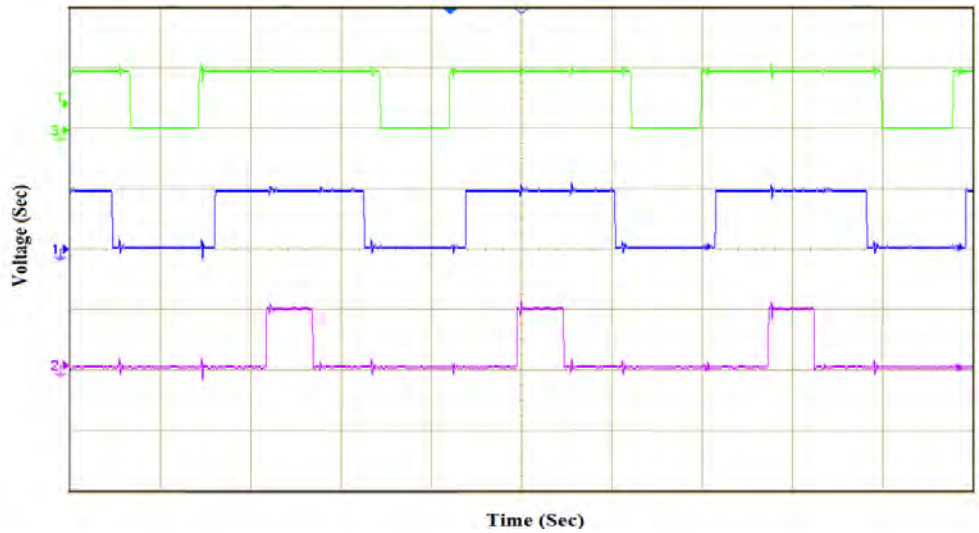

Fig. 17 Pulse generation using SVPWM

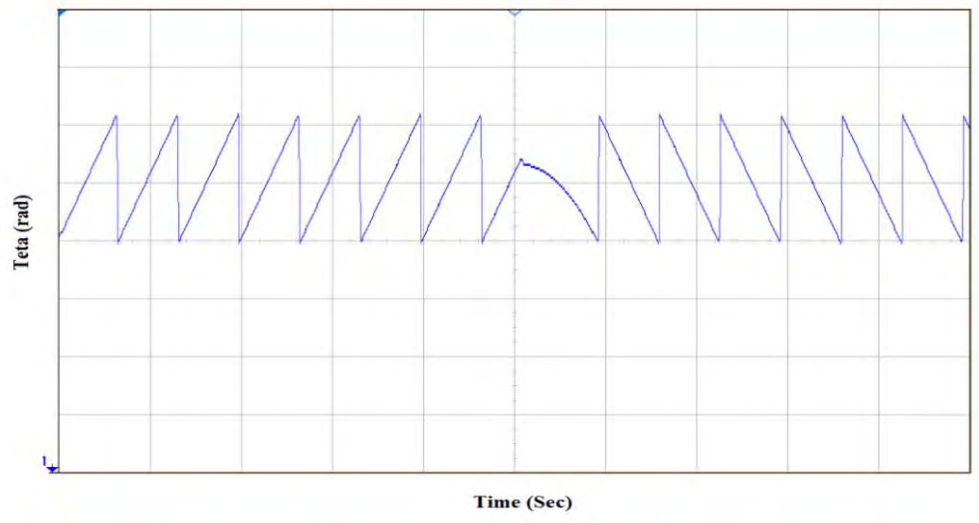

Y AXIS : 80 rad/div, X AXIS : 50ms/div

Fig. 18 Rotor flux angle (Forward and Reverse)

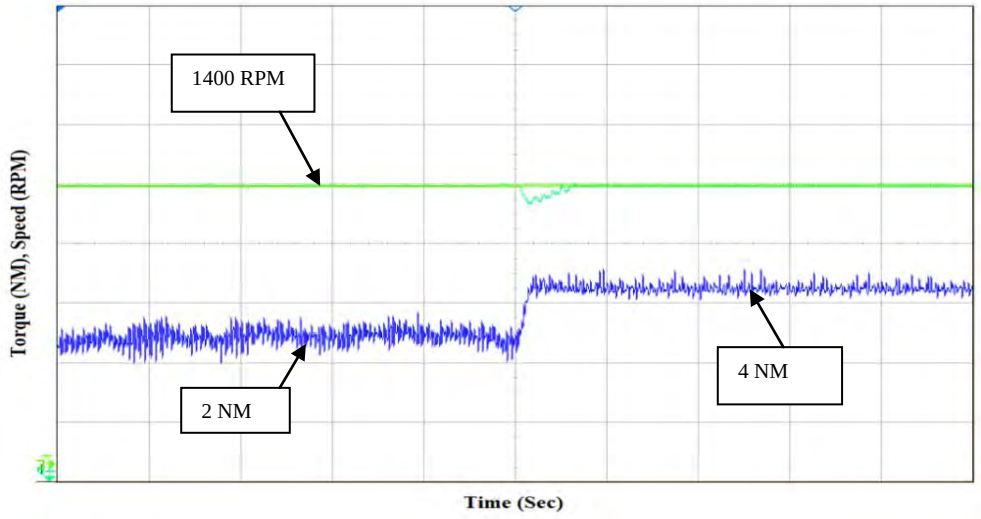

Fig. 19 Speed and torque curve when load is applied (with ref. speed)

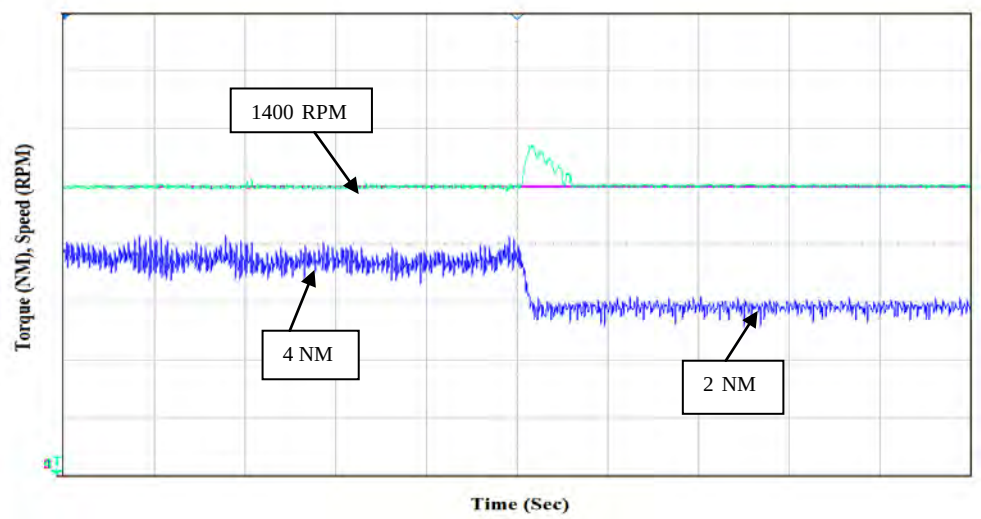

Fig. 20 Speed and torque curve when load is removed (with ref. speed)

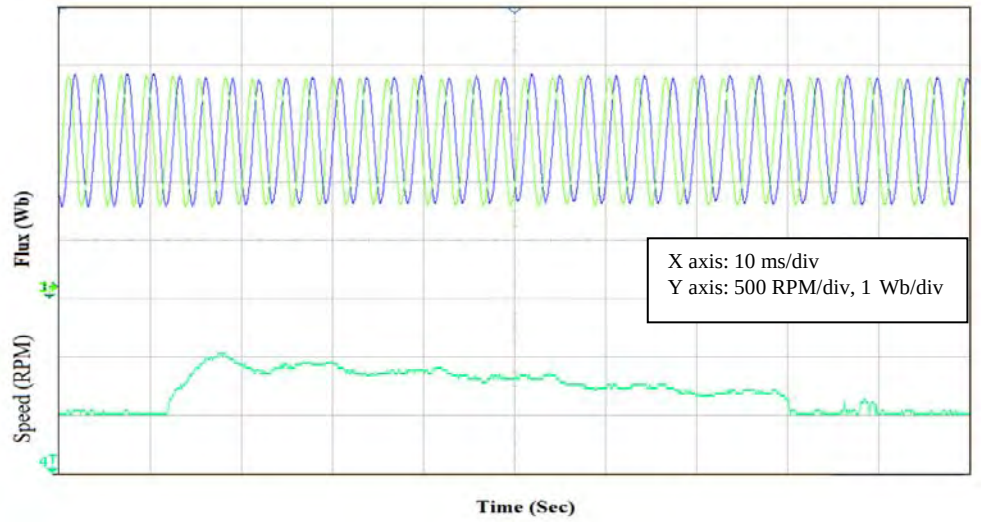

Fig. 21 $Ø_d$, $Ø_q$ and speed characteristics when load is applied

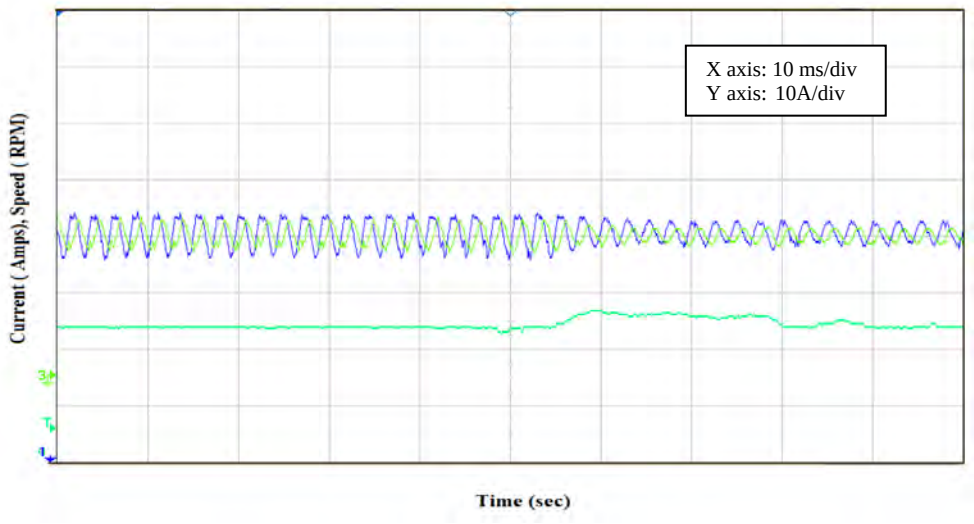

Fig. 22 I_d, I_q and speed characteristics when load is applied

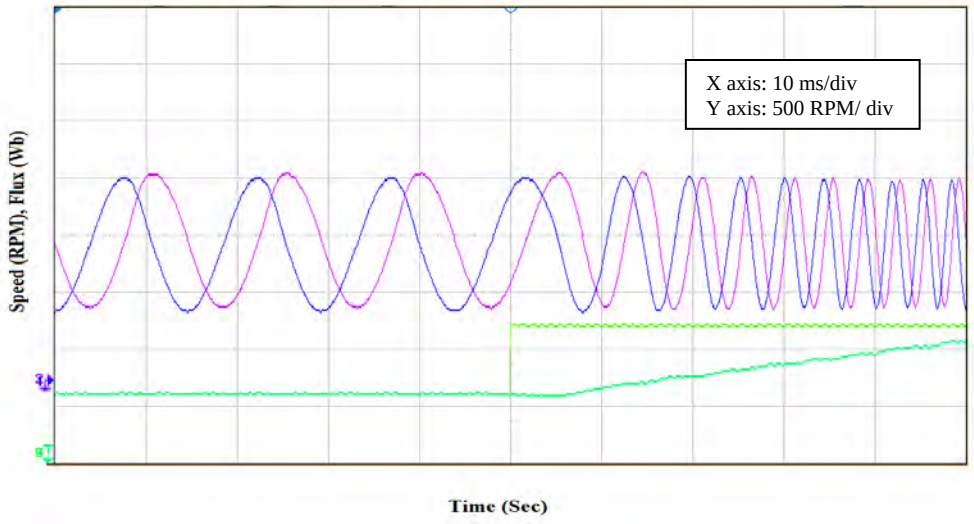

Fig. 23 Speed, $Ø_d$, $Ø_q$ without load in classical DTC

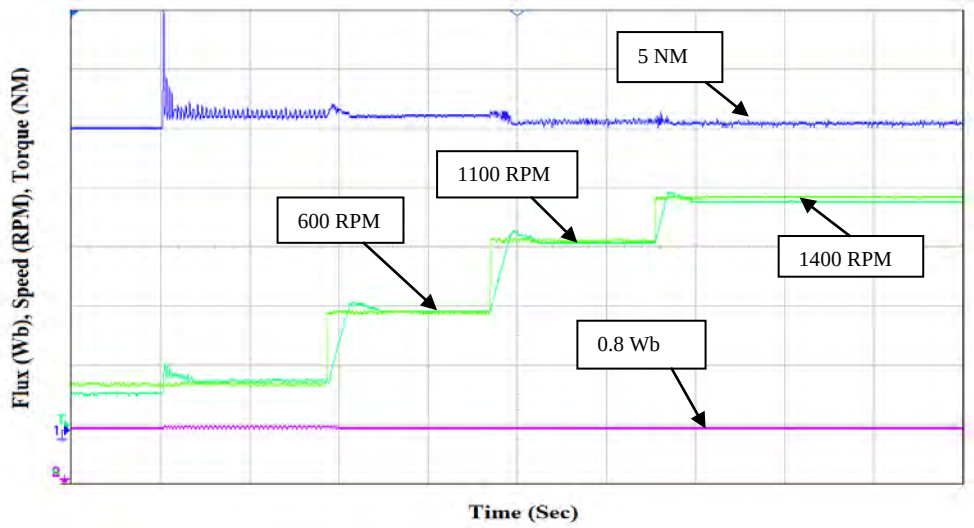

Fig. 24 Flux, torque and speed response in classical DTC

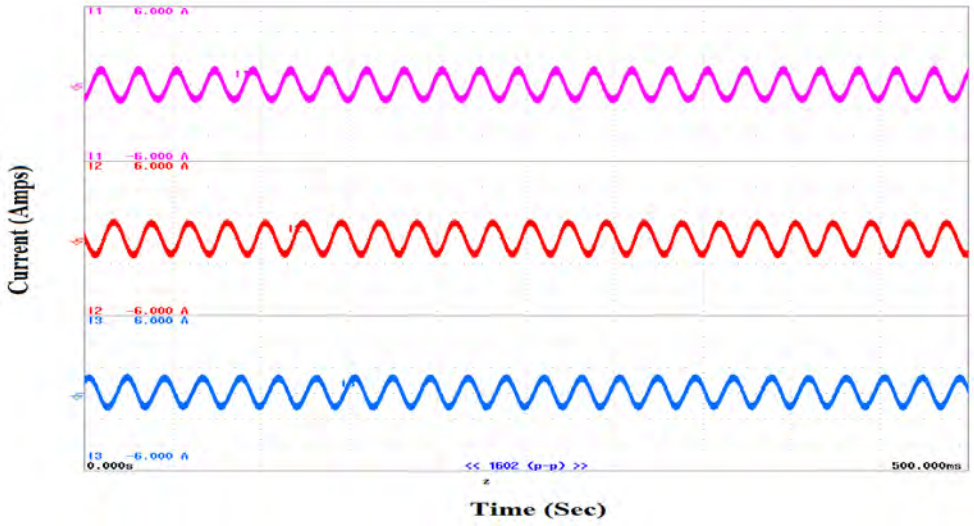

Fig. 25 Full load current of induction motor

Fig. 20 shows the speed and torque characteristics of the induction motor when the load is suddenly removed, the torque decreases suddenly and the speed increseas and settles down at the set speed in 2 seconds. Fig. 21 shows the $Ø_d$, $Ø_q$ and speed characteristics when load is applied to the induction motor. Fig. 22 shows the change in magnitude of I_d, I_q and speed curves when load is applied to the rotor shaft. Fig. 23 shows the Speed, $Ø_d$, $Ø_q$ characteristics of classical DTC induction motor. When sudden load is applied to the rotor shaft, the frequency of the $Ø_d$ and $Ø_q$ changes and hence the flux is calculated as shown. Fig. 24 shows the flux, torque and speed response of induction motor using classical direct torque control. The speed of the induction motor is set at 600 RPM, 1100 RPM and 1400 RPM at certain intervals and their corresponding settling speed is mentioned. Flux of the induction motor is 0.8Wb. Fig. 25 shows the stator current of the induction motor, when the motor is at full-load and measures 1.8 A of current. Direct torque control technique are used by many researchers because of its wide area applications with various ac machine types as induction motor, PMSM, PM Brushless, and reluctance motor.

VI. CONCLUSION

The aim of the paper was to propose a low-cost, phase-current reconstruction algorithm for a PV powered direct torque control three-phase induction motor. The hardware implementation is done with Spartan 3E FPGA Kit.The number of sensor is reduced by using phase-current reconstruction algorithm. The maximum dc power can be obtained from the PV array by using the "HILL CLIMBING" algorithm to the switches of the current fed full bridge boost dc-dc converter. The advantage of using dc-dc converter here is that all of the parasitic capacitances and inductances are included in the resonant or filter circuits and the system does not generate parasitic oscillations and is without any uncontrolled high voltage and current spikes. The conclusion is that the whole performance of the system is improved compared to a vector control of induction motor. The settling time of the speed and ripples present in the torque are reduced hence DTC method are preferred than vector control.

REFERENCES

[1] T. Muthamizhan and R. Ramesh, "Design and Simulation of PV driven three phase Induction motor", International Review on Modelling and Simulations, vol. 6, no. 2, pp. 412-418, April. 2013.
[2] R. Arivazhagan and S. L. Prakash, "Analysis of current-fed full bridge converter with modified auxiliary circuit", Proceedings of the international Conference on in Recent Advancements in Electrical, Electronics and Control Engineering, pp. 357-362, 2011.
[3] G.S. Buja and M.P. Kazmierkowski, 'Direct torque control of PWM inverter-fed AC motors - A survey", IEEE Transactions on Industrial Electronics, vol. 51, no. 4, pp. 744-757, 2004.
[4] R.Y. Chen, T.J. Liang, J.F.Chen, R.L. Lin and K.C. Tseng, 'Study and implementation of a current-fed full-bridge boost DC–DC converter with zero-current switching for high-voltage applications', IEEE Transactions on Industry Applications, vol. 44, no. 4, pp. 1218-1226, 2008.
[5] A. Choudhury and K. Chatterjee, 'Speed sensor less direct torque controlled induction motor drive with constant switching frequency operation', Proceedings of the international conference on Energytech,2011, pp. 1-6.
[6] E.E. El-kholy, R. Kennel, A. El-refaei, S.A. El-Latif and F. Elkady, "Robust Space–Vector Current Control for Induction Motor Drives', Journal of Electrical Engineering, vol. 57, no. 2, pp. 61–68, 2006.
[7] T. Esram and P. L. Chapman, "Comparison of Photovoltaic Array Maximum Power Point Tracking Technique", IEEE Transactions on Energy Conversion, vol. 22, no. 2, pp. 439-449, 2007.
[8] N. Femia, G. Petrone, G. Spagnuolo, and M.Vitelli, "Optimization of perturb and observe maximum power point tracking method", IEEE Transactions on Power Electronics, vol. 20, no. 4, pp. 963-973, 2005.
[9] S.B. Kjaer, "Evaluation of the "Hill Climbing" and the "Incremental Conductance", Maximum Power Point Trackers for Photovoltaic Power System", IEEE Transactions on Energy Conversion, vol. 27, no. 4, pp. 922-929' 2012.
[10] A. Mathew and A. I. Selvakumar, "MPPT based stand-alone water pumping system', Proceedings of international conference on Computer, Communication and Electrical Technology, 2011, pp. 455-460.

[11] S. R. Maturu and A. Vujji, "SVPWM Based Speed Control of Induction Motor Drive with Using V/F Control Based 3-Level Inverter", VSRD International Journal of Electrical, Electronics & Communication Engineering, vol. 2, no. 7, pp. 421-437, 2012.
[12] N. Pimkumwong, A. Onkrong and T. Sapaklom, "Modeling and Simulation of Direct Torque Control Induction Motor Drives via Constant Volt/Hertz Technique", Procedia Engineering, 2012, vol. 31, pp. 1211-1216.
[13] B. Rashidi and M. Sabahi, "High Performance FPGA Based Digital Space Vector PWM Three Phase Voltage Source Inverter", International Journal of Modern Education and Computer Science, vol. 5, no. 1, pp. 62-71' 2013.
[14] A. Sivakumar, T. Muthamizhan, N. O. Gunasekhar & R. Ramesh, "A Novel Sensorless Speed Control Strategy of Induction Motor Based on Vector Control", International Review of Electrical Engineering, vol. 8, no. 4, pp. 1211-1217, Aug. 2013.
[15] B. Singh, S. Jain and S. Dwivedi, "Direct Torque Control Induction Motor Drive with Improved Flux Response" Advances in Power Electronics, vol. 2012, pp. 1-11, 2012.
[16] M.A. Vitorino, M.B. de Rossiter Correa, C.B. Jacobina and A.M.N. Lima, "An Effective Induction Motor Control for Photovoltaic Pumping", IEEE Transactions on Industrial Electronics, vol. 58, no. 4, pp. 1162-1170, 2011.
[17] Y. Yao, P. Bustamante R.S. Ramshaw, "Improvement Of Induction Motor Drive Systems Supplied By Photovoltaic Arrays With Frequency Control", IEEE Transactions on Energy Conversion, vol. 9, no. 2, pp. 256-262,1994.
[18] K.K. Yoon and S.H. Kim, "Sensorless Speed Control of Induction Motor by Direct Torque Control with Numerical Model", Journal of the Korean Society of Marine Engineering, vol. 36, no. 6, pp. 830-836, 2012.
[19] K. Zhou and D. Wang, "Relationship Between Space-Vector Modulation and Three-Phase Carrier-Based PWM: A Comprehensive Analysis', IEEE Transactions on Industrial Electronics, vol. 49, no. 1, pp. 186-196, 2002.
[20] L. Zhou and X. Ruan, "A zero-current and zero-voltage-switching PWM boost full-bridge converter', Proceedings of thirty-fourth annual conference in Power Electronics Specialist Conference, 2003, vol. 2, pp. 957-962.